

Original Research

# Constructing the *in vitro* culture system of the sika deer (*cervus nippon*) antler periosteal cell to detect its function on antler regeneration

Guanning Wei<sup>1,2</sup>, Tao Qin<sup>3</sup>, Xunsheng Li<sup>2</sup>, Zhen Wang<sup>2</sup>, Yusu Wang<sup>2</sup>, Qing Guan<sup>2</sup>, Wanwan Shi<sup>2</sup>, Liuwei Xie<sup>2</sup>, Shoujing Zhao<sup>1,\*</sup>, Hongmei Sun<sup>2,\*</sup><sup>1</sup>School of Life Sciences, Jilin University, 130012 Changchun, Jilin, China<sup>2</sup>Institute of Special Wild Economic Animals and Plants, Chinese Academy of Agricultural Sciences, 130112 Changchun, Jilin, China<sup>3</sup>School of Ecology and Environment, Northwestern Polytechnical University, 710072 Xi'an, Shaanxi, China\*Correspondence: [swgc@jlu.edu.cn](mailto:swgc@jlu.edu.cn) (Shoujing Zhao); [sunhongmei@caas.cn](mailto:sunhongmei@caas.cn) (Hongmei Sun)

Academic Editor: Brenda M. Alexander

Submitted: 18 November 2021 Revised: 20 January 2022 Accepted: 25 January 2022 Published: 17 February 2022

## Abstract

Periosteum is essential for bone regeneration and damage repair in mammals. Most species of deer family (Cervidae) develop two kinds of special periosteum, antler periosteum and pedicle periosteum, both supporting the complete regeneration of antler. Antler is the bone organ with the fastest growth rate in mammals. Along with the fast growth of antler, its external tissues such as blood vessels, nerves and the covering skin also grow rapidly. Currently, it is still unclear whether antler periosteum contributes to the fast growth of antler and how. It is also unclear why the regenerative capacity of antler periosteum is weaker than that of pedicle periosteum. In this study, the *in vitro* culture system for antler periosteal cells (AnPC) was constructed for the first time using the mid-beam antler periosteum during antler fast-growth period. According to our results, the cultured AnPC expressed classical MSC markers, consistent with the pedicle periosteal stem cells (PPSC). However, the fluorescence intensities of the MSC markers on AnPC were significantly weaker than those on PPSC. In addition, AnPC showed much lower proliferation rates than PPSC. The proliferation rates of the AnPC also gradually decreased after successive passages, while the proliferation rates of the pedicle periosteal stem cells remained unchanged. These findings may partially explain the weaker regenerative capacity of antler periosteum. Further comparative global gene analysis revealed clearly the different gene expressed patterns between AnPC and PPSC. AnPC may mainly function on promoting angiogenesis, nerve growth and intramembrane bone formation during antler regeneration, whereas PPSC may primarily be involved in androgen signaling receptor pathway and PI3K-Akt signaling pathway and function on maintaining stem cell renewal.

**Keywords:** sika deer; antler periosteum; pedicle periosteum; antler regeneration; antler rapid growth

## 1. Introduction

Periosteum is a thin layer of vascularized tissue lining the outer bone surface. It plays an essential role in bone regeneration and damage repair in mammals [1–8]. Most species from the deer family (Cervidae) possess two special types of periosteum—the pedicle periosteum and the antler periosteum, making them unique among mammals in terms of regenerative capacity. The pedicle periosteum and the antler periosteum support the complete regeneration of the antler [9–11]. The pedicle periosteum cover the pedicles, which are two symmetrically permanent bony protuberances on the deer frontal bone (Fig. 1A). Pedicles are the antecedents to the formation of antlers. Most deer species begin to develop pedicles as the fawns approach puberty [12]. When the pedicles reach the species-specific maximum height, the first antlers generate spontaneously from the apices of the pedicles [13]. Then the deer's antlers enter a testosterone level-dependent regenerative cycle after casting every year [12,14,15], and the pedicles increase in diameter and decrease in length gradually to support antler regeneration [16]. It has been well recognized that pedicle periosteum induces antler regeneration. The pedicle

periosteum is naturally consumed partly to regenerate new antler every year [12,14,17]. In comparison, the antler periosteum covering the regenerative antler shaft (Fig. 1A) are not consumed naturally. When an antler is amputated artificially or by accident, the antler periosteum can trigger self-regeneration of the antler under low androgen levels [10]. Previous studies have reported that the regenerative capacity of the antler periosteum is significantly weaker than that of the pedicle periosteum [10,11,18]. The size of the antler regenerated from the antler periosteum is significantly smaller than that from the pedicle periosteum [10,11,18,19]. In addition, the antler periosteum gradually loses regenerative capacity through successive epimorphic experiments, whereas the pedicle periosteum still maintains [18,19].

Bone regeneration mainly relies on the presence and activation of the periosteal stem cells within the periosteum [2,20,21]. Previous studies have shown that cultured pedicle periosteal cells express classical mesenchymal stem cell (MSC) markers and maintain multiple differentiation potentials [22–24], same as the reported adult periosteal stem cells contributing to bone regeneration [2,21,25–27]. In



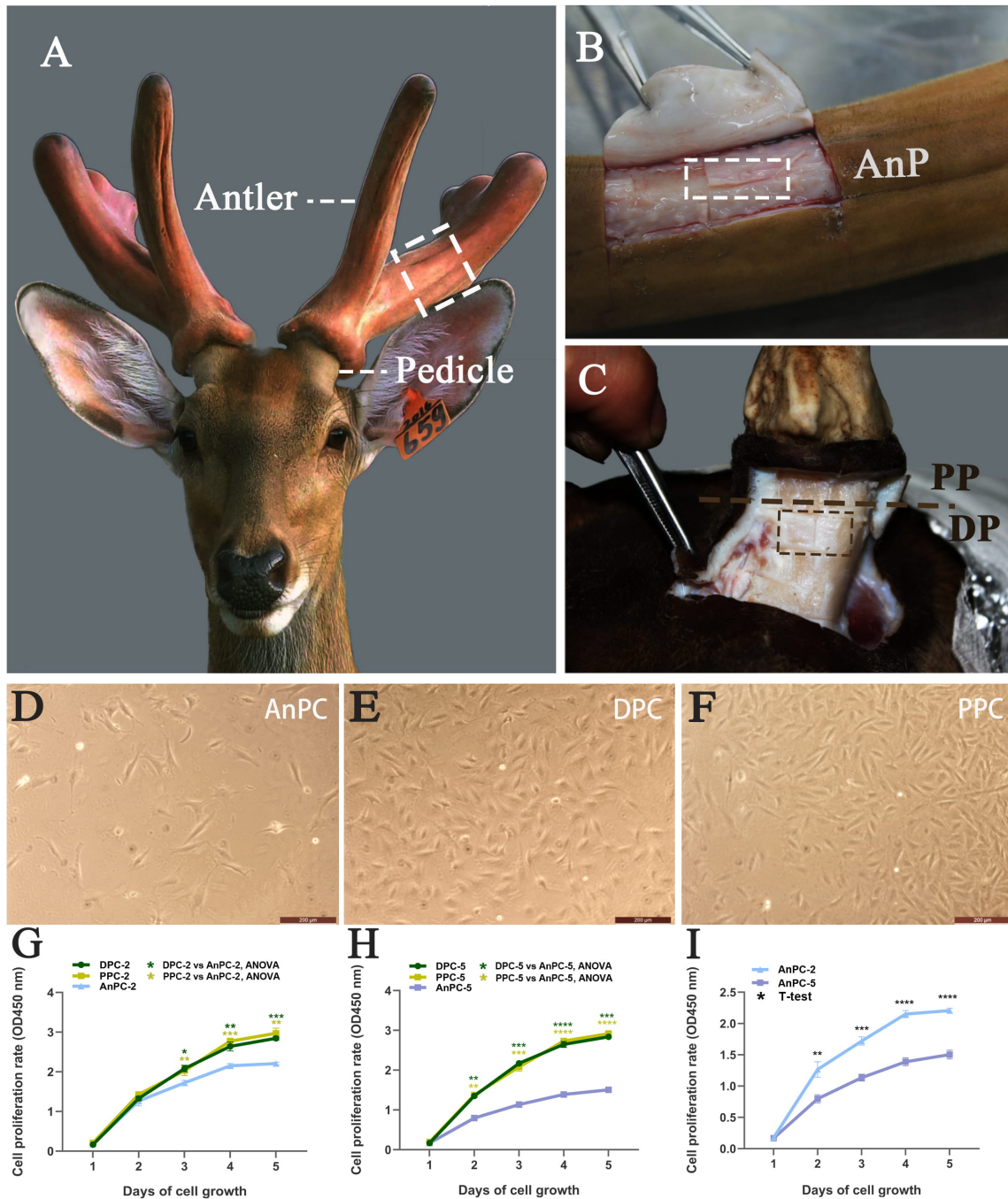


**Fig. 1. Tissue extraction and cell culture for sika deer antler periosteum and pedicle periosteum.** (A) The pedicle and the regenerative antler outgrow from the pedicle. The dotted box denotes the location where the antler periosteum were harvested. (B) The antler periosteal tissues (AnP) harvested for primary cell culture, denoted by the white dotted box. (C) The pedicle periosteal tissues (DP and PP) harvested for primary cell culture, denoted by the brown dotted box. (D) The sub-cultured antler periosteal cells (AnPC) showing monolayer polygonal and fibroblastic morphology in DMEM/FBS, bar = 200  $\mu\text{m}$ . The pedicle periosteal stem cell (E) DPC and (F) PPC in DMEM/FBS showing same monolayer polygonal and fibroblastic morphology, red bar = 200  $\mu\text{m}$ . (G–I) Comparison of cell proliferation on (G) the second-passage DPC, PPC and AnPC, one-way ANOVA, (H) the fifth-passage DPC, PPC and AnPC, one-way ANOVA, and (I) the second-passage AnPC and the fifth-passage AnPC, paired *t*-test, through Cell Counting Kit-8 assay respectively. Y-axis represents the OD values at a wavelength of 450 nm. X-axis represents the period of cell growth. \*\*\*\* $p < 0.0001$ , \*\*\* $p < 0.001$ , \*\* $p < 0.01$ , \* $p < 0.05$ .

the early stage of antler regeneration, the distal pedicle periosteum initially increase in thickness following the cast of the ossified antlers [25,27] and migrate towards the center of the cast surface to form blastema. The blastema finally forms perichondrium, which covers the antler tip and connects proximally with the antler periosteum as the new antler regenerates [28,29]. The reserve mesenchyme layer, precartilaginous layer, transition layer and cartilage layer localize below the perichondrium longitudinally, with immunohistochemically localized MSC markers as well [30]. In comparison, the characteristic of antler periosteum has been rarely reported. The factors leading to the weaker regenerative capacity of the antler periosteum, compared to the pedicle periosteum, are also waiting to be detected [28,29,31].

Histologically, deer antlers and pedicles demonstrate similar growth patterns, with elongation via modified endochondral ossification and latitudinal growth via intramembranous ossification [25–27,32]. However, the growth rates of the regenerative antlers and the pedicles are strikingly different. The elongation of the regenerative antler follows a typical S-shape growth curve. In the first month to six weeks after regeneration, antler longitudinal growth is relatively slow. Throughout the next 60–80 days there follows a period of rapid exponential growth that slows as autumn approaches. During the fast-growth period, the average growth rate of a sika deer antler can reach up to 1.14 cm/day [17]. For some giant deer species, such as elk (moose), the average growth rate of an antler will elongate by more than 2 cm/day [33]. This rate of bone formation represents the fastest described in the mammalian kingdom [16]. In contrast, pedicles demonstrate relatively constant growth rate. The average growth rate of a pedicle is 0.4 mm/day [26], similar to that of human femur (0.32 mm/day during embryonic development [34] and 0.42 mm/year from three to sixteen years of age [35,36] on average). Along with the fast growth of the antler, the coordinated regeneration of multiple tissue types such as blood vessels, nerves and the covering skin also grow rapidly. Whether the antler periosteum contributes to the fast growth of antler remains unknown and needs further investigation.

In this study, we conducted the *in vitro* culture system of the antler periosteum for the first time. In addition, we found the antler periosteal cells (AnPC) expressed weaker MSC markers and decreased proliferation rates than pedicle periosteal stem cells (PPSC), likely leading to the weakened regenerative capacity of the antler periosteum. To further reveal the functions of AnPC in antler regeneration, the transcriptome analysis was conducted to compare the gene expression patterns between AnPC and PPSC. The candidate genes and regulating pathways contributing to fast growth of the antler were predicted and verified through real-time PCR analysis.

## 2. Material and methods

### 2.1 Tissue collection

The antler periosteal tissues (AnP; Fig. 1A,B) were collected from the mid-beam of the three commercially harvested 2-branch velvet antlers, taken from three male sika deer (*Cervus nippon*, 2–3 years old) during the antler fast-growth period in July (northern hemisphere). Immediately after sawed, the fresh antlers were taken back to the lab for sterilization, using 75% ethanol and iodine solution. The velvet skin was cut to expose the antler periosteum, which was cut into 0.3 cm × 2 cm strips, then tore off from the antler shaft and placed into the phosphate buffer saline (PBS) with 5× penicillin-streptomycin (03-031-5B, BI, Beit Haemek, Israel) solution for wash. The two types of pedicle periosteal tissues (DP and PP; Fig. 1C) were collected in November from three farmed male sika deer with ages of 2–3 years old, when antler became ossified. The harvest of periosteal tissues followed the tissue collection methods that have been previously described [37]. Specifically, the DP tissues (n = 3 each) were extracted from the proximal two-thirds of pedicle periosteum (Fig. 1C), a region where the periosteum loosely attaches to the skin immediately after slaughter. The cells that reside in DP are postulated to stay in dormant stem cell status [22]. The PP tissues (n = 3 each) were extracted from the distal third of periosteum (Fig. 1C), a region where the periosteum firmly attaches to the skin. The cells that reside in PP are postulated to stay in activated stem cell status [22].

### 2.2 Cell culture

The primary cell cultures for antler periosteum and pedicle periosteum were conducted according to established protocols [23,38]. After washing by three consecutive PBS washes, the periosteum strips were digested in Dulbecco's Modified Eagle's Medium (DMEM, 11965092, Gibco, Grand Island, NY, USA) containing collagenase D (150 units/mL, 11088858001, Roche, Agawam, MA, USA). After removing the collagenase, the digested complexes were cultured in DMEM medium containing 10% fetal bovine serum (10099141, Gibco), 100 mg/mL of streptomycin and 100 units/ml of penicillin (03-031-5B, BI) in a humidified atmosphere with 5% CO<sub>2</sub> at 37 °C. The primary cultured cells were trypsinized and transferred into T75 culture flasks (430641, Corning®, Canton, NY, USA) when reaching sub-confluent. Half the amount of the sub-cultured cells was used for the following experiments when cell density reached 80% confluence. The rest cells were saved in liquid nitrogen for future use. AnPC are referred to as the cells cultured from the periosteum of antler mid-beam, DPC are referred to as the stem cells cultured from proximal two-thirds of the pedicle periosteum, and PPC are referred to as the stem cells cultured from the distal third of periosteum, respectively.

### 2.3 Cell counting Kit-8 assay

The comparison of cell proliferation rates between AnPC, PPC and DPC was conducted using Cell Counting Kit-8 (C0037, Beyotime, Shanghai, China), according to the manufacturer's instructions. Three biological replicates were performed for AnPC, DPC and PPC, respectively. The 50 cells from each cell type were seeded into each well of a 96-well plate with a volume of 100  $\mu$ L medium. Cells were cultured for 24 h. After adding 10  $\mu$ L CCK-8 reagent to each well, the plate was incubated for 2 h at 37 °C and 5% CO<sub>2</sub>. The absorbance of each well was measured at 450 nm and the optical density (OD) was determined via a microplate reader. The test time points were set as the 1st day, 2nd day, 3rd day, 4th day and 5th day. The one-way ANOVA test and paired *t*-test were used to calculate the differences between samples and *p* value < 0.05 was considered as statistically significant. GraphPad Prism (v. 8.2.0, San Diego, CA, USA) was used to analyze data.

### 2.4 Mesenphere formation assay

The sub-cultured AnPC, DPC and PPC in DMEM (11965092, Gibco)/FBS (10099141, Gibco) were collected using trypsin, when they reached to 80% confluence. The 150 cells were seeded into each well of the 24-well plate and each treatment was performed in triplicate. Cells were maintained in the serum-free mesenchymal stem cell (MSC) medium (T310jv, Yuanpei, Shanghai, China) with 1 $\times$ penicillin-streptomycin solution (03-034-1B, BI) in a humidified atmosphere with 5% CO<sub>2</sub> at 37 °C. The medium was refreshed every 2 days.

### 2.5 Immunofluorescence staining

The sub-cultured AnPC, DPC and PPC were fixed under 4% (wt/vol) paraformaldehyde fixation for 10 min. For intracellular proteins, cells were permeabilized for 5 min using PBS with 0.3% Triton X-100 (T8787, Sigma). Blocking was performed for 30 min using 3% (wt/vol) Bovine Serum Albumin in PBS. The primary antibodies including rabbit anti-CD73 (1:300; SantaCruz, Santa Cruz, CA, USA), rabbit anti-CD90 (1:300; Bioss, Beijing, China), rabbit anti-CD105 (1:300; Thermo, Agawam, MA, USA) and rabbit anti-Nestin (1:300; GeneTex, Irvine, CA, USA) were left overnight at 4 °C. In the next day, the primary antibodies were washed off using three consecutive PBS washes. The secondary antibody, Alexafluor 594 goat anti-rabbit (1:1000; Thermo, Agawam, MA, USA) was applied for 1 h at room temperature. The nuclei of cells were counterstained with DAPI (C1005, Beyotime, Shanghai) for 5 min at room temperature after removing the secondary antibody using three consecutive PBS washes. The coverslips were mounted using anti-fade reagent and the cells were visualized on a Zeiss Exciter fluorescent microscope. The fluorescence intensity of the markers was calculated by ImageJ software (v.1.53k, Bethesda, MD, USA) and compared through one-way ANOVA by GraphPad Prism (v. 8.2.0).

The specific information on all the antibodies used is listed in **Supplementary Table 1**.

### 2.6 De novo transcriptome analysis

After decanting the culture medium from the T75 flasks and washing by PBS twice, the AnPC, DPC and PPC of second passages were trypsinized, centrifuged and re-suspended in PBS at 4 °C. Total RNA was isolated and purified using RNeasy mini kit 50 (151043752, Qiagen, Germantown, MD, USA), according to the manufacturer's procedure. RNA quality was confirmed through Agilent 2100 Bioanalyzer (Agilent RNA 6000 Nano Kit) with a minimum RNA integrity number of 7.6. 1  $\mu$ g per RNA sample was used to construct library (Illumina TruSeq Library Preparation Kit v3). The libraries were sequenced using an Illumina HiSeq Xten sequencing platform (BGI, Shenzheng, China) and 150 bp paired-end reads were generated. The Trinity (v. 2.0.6, Cambridge MA, 02142, USA) [39] was used to perform de novo assembly to generate transcripts with clean reads. The transcripts were clustered and filtered to generate unigenes using the Tgicl (v. 2.0.6, Rockville, MD, USA) [40]. The Blast (v. 2.2.23, Bethesda MD, USA) [40] was used to align unigenes to NT, NR, KOG, InterPro, KEGG and SwissProt database for the annotation. The unigenes annotated by SwissProt database were finally selected for mapping to the clean reads using Bowtie2 (v. 2.2.5, College Park, MD, USA) [41]. The gene expression level and FPKM were calculated with RSEM (v. 1.2.12, Charlestown, MA, USA) [42].

### 2.7 Bioinformatics analysis on gene expression pattern and differentially expressed genes

The gene expression patterns of AnPC, DPC, and PPC were compared through PCA analysis and hierarchical clustering analysis, performed through the MetaboAnalyst (v. 4.0, Quebec, Quebec, Canada) [43]. The differentially expressed genes (DEGs) were identified using DESeq2 R package (v2.1.18, Boston, MA, USA) [44] and visualized in volcano plot using GraphPad Prism 8 (v. 8.2.0). The adjusted *p* value  $\leq$  0.01 and  $|\log_2\text{foldchange}| \geq 1$  were set as the threshold for significantly differential expression. The Venn analysis was performed to calculate the numbers of DEGs among AnPC, DPC and PPC using Excel. The GO enrichment analysis and the KEGG pathway enrichment analysis on the selected DEGs were performed using David v6.8 [45] and visualized using ggplot2 R package. The Cytoscape (v. 3.7.1, Bethesda, MD, USA) [46] was used to perform the gene network analysis (*p* value  $\leq$  0.01).

### 2.8 Quantitative real-time PCR (qRT-PCR) analyses

After the cells were briefly washed three times by PBS, the total RNAs of AnPC, DPC and PPC were isolated and purified using RNeasy mini kit 50 (151043752, Qiagen, Germantown, MD, USA), according to the manufacturer's instructions. RNA was quantified by measuring op-

tical absorbance at 260 nm (Pro2000, Tecan, Switzerland) and a 200 ng was reverse transcribed to cDNA using Prime-Script™ RT reagent Kit (RR047A, Takara, Shiga, Japan) and oligo dT primers following the manufacturer's instructions. Real-time PCR was performed using SYBR green I Master mix (4707516001, Roche) on an Applied Biosystems 7300 Real-Time PCR System. GAPDH were used in each reaction as a baseline control. The fold changes were calculated using the delta-delta CT algorithm, relative to GAPDH. The one-way ANOVA test was used to calculate the differences among AnPC, DPC and PPC. Three biological replicates were performed for each gene of interest and  $p$  value  $< 0.05$  was considered as statistically significant. GraphPad Prism (ver. 8.2.0) was used to analyze data. The primer information is listed in **Supplementary Table 2**.

### 3. Results

#### 3.1 Construction of the *in vitro* culture system for Sika deer antler periosteal cells

To investigate whether antler periosteal cells (AnPC) demonstrate the same characteristics as the pedicle periosteal stem cells (PPSC), we used the same culture condition for the pedicle stem cells to construct an *in vitro* culture system for the sika deer AnPC. The antler periosteal tissues (AnP) were first isolated from antler mid-beam periosteum during antler fast-growth period (Fig. 1A,B), and then cultured in the DMEM/FBS medium. The proximal two-thirds of the pedicle periosteum (DP) and the distal third of the pedicle periosteum (PP) were also harvested separately (Fig. 1C) and cultured in the same culture condition as control groups. All the three types of periosteal cells began to migrate out from the attached tissues within 24–48 hours. The sub-cultured antler periosteal cells (AnPC, Fig. 1D) demonstrated the same polygonal fibroblastic morphology as PPSC (DPC, Fig. 1E and PPC, Fig. 1F). From the CCK-8 test results, the second passages of PPC and DPC showed significantly more rapid cell expansion rates than that of AnPC since the third day, while PPC and DPC showed the same proliferation rates (Fig. 1G). Similarly, the fifth passages of PPC and DPC also demonstrated significantly faster cell expansion rates than the fifth passages of AnPC since the second day, while PPC and DPC showed the same proliferation rates (Fig. 1H). There was no change of proliferation rates between the second and the fifth passages of PPC and DPC. However, the proliferation rate significantly declined from the second passages to the fifth passages of AnPC (Fig. 2F). Our results suggested that PPC and DPC proliferated much faster than AnPC. During successive passages, PPC and DPC kept the same proliferation rates, whereas AnPC showed a gradually declined proliferation rate.

#### 3.2 Detecting the characteristics of antler periosteal cells

To evaluate the characteristics of AnPC, the classical mesenchymal stem cell (MSC) markers expressed by cul-

tured PPSC [23] were used in this study. The results showed AnPC were also positive to CD105, CD90, and CD73, consistent with DPC and PPC (Fig. 2J–L). However, compared to the strong expression of the MSC markers on PPSC, the fluorescence intensities of all MSC markers on AnPC were significantly weaker (Fig. 2Q). The percentage of the positive cells of AnPC were also significantly lower than that of DPC or PPC (**Supplementary Table 3**). Note that there was no significant expression difference of the three markers between DPC and PPC. In addition, we detected all AnPC, DPC and PPC with nestin expression (Fig. 2M1–3) and mesosphere-forming capability (Fig. 2N1–3, O1–3, P1–3), which were typical phenotypes of the neural-crest-derived stem cells [47–52]. Therefore, the AnPC, PPC and DPC likely shared the same neural crest origin. Interestingly, we also found the fluorescence intensities of all the MSC markers on DPC, PPC and AnPC gradually increased as the mesospheres clustered from the monolayer cells (Fig. 2A–I). The expressions of CD73, CD90 and CD105 all became strengthened as DPC, PPC, and APC aggregated into clusters (Fig. 2A–I left panels) and reached highest when mesospheres formed (Fig. 2A–I right panels). Fig. 2N–P show the steps of the DPC, PPC and APC mesosphere formation from the monolayer DPC, PPC and APC when the culture medium was changed from DMEM/FBS to serum-free MSC medium.

#### 3.3 Transcriptome analysis reveals the functions of antler periosteal stem cells

##### 3.3.1 Assembly and annotation of unigenes

To reveal the gene profile of the antler periosteal stem cell lineage to uncover its function on antler regeneration, comparative transcriptional analysis was applied to AnPC, DPC and PPC. A total of 404.75 million (60.72 Gb) bases were first generated on the Illumina HiSeq sequencing platform. After assembling all samples together and filtering the abundance, 107,389 unigenes were generated. The total length, average length, N50, and GC content of Unigenes are 146,306,853bp, 1,362bp, 3,362bp and 51.09% respectively. The unigenes were then aligned with seven functional databases to acquire 50,635 (NR: 47.15%), 101,389 (NT: 94.41%), 43,779 (Swissprot: 40.77%), 37,858 (KOG: 35.25%), 41,439 (KEGG: 38.59%), 14,601 (GO: 13.60%) and 34,581 (InterPro: 32.20%) annotated unigenes. Finally, the 43,779 unigenes (40.77%) annotated via SwissProt were selected for the downstream functional analysis in this study ( $p$  value  $\leq 0.01$ ).

##### 3.3.2 Antler periosteal cells demonstrate differential gene expression compared to pedicle periosteal stem cells

The PCA analysis was performed to obtain the large-scale patterns of gene expression across AnPC, DPC and PPC, using the 43779 unigenes (Fig. 3A). PC1 explains 89.9 % of the overall variation so that it could represent the overall trend. On PC1, the distance between AnPC and DPC/

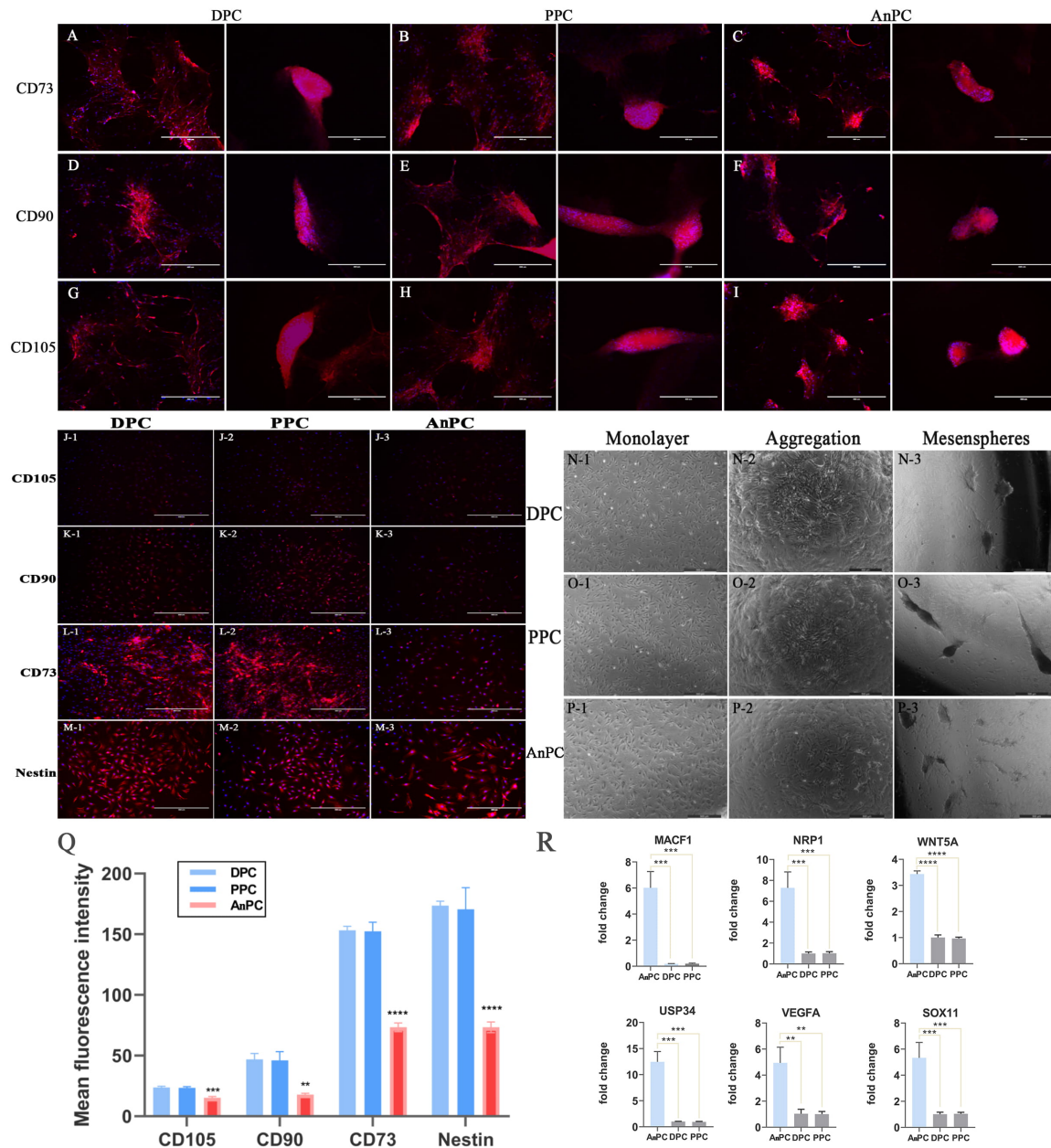


**Fig. 2. Detecting the stem cell characters of AnPC.** (A–I) The expression of CD73, CD90 and CD105 on (A, D, J) DPC, (B, E, H) PPC and (C, F, I) AnPC when clusters aggregate (left panels) and when mesenspheres form (right panels), respectively, bar = 400  $\mu\text{m}$ . Note, the expressions of all the markers on DPC, PPC and AnPC all become strengthened as clusters form and reach highest when mesenspheres form. (J–M) The expression of (J) CD105, (K) CD90, (L) CD73 and (M) nestin on monolayer DPC (left panels), PPC (middle panel) and AnPC (right panels), respectively, bar = 400  $\mu\text{m}$ . (N–P) The (N) DPC, (O) PPC and (P) AnPC mesensphere formation from the monolayer DPC, PPC and AnPC respectively when the culture medium was changed from DMEM/FBS to serum-free MSC medium (N–P left panels). The sub-culture DPC, PPC and AnPC of the second passage in DMEM/FBS demonstrate monolayer morphology (N–P middle panels). The monolayer DPC, PPC and AnPC aggregate into cluster-like or net-like strands at high cell density after the culture medium is changed into serum-free MSC medium (N–P right panels). The DPC, PPC and AnPC finally aggregate into mesenspheres of 150–200  $\mu\text{m}$  diameter, bar = 500  $\mu\text{m}$ . (Q) Comparison of fluorescence intensities of the MSC markers on DPC, PPC and AnPC. Y-axis represents the mean fluorescence intensity of the MSC markers. X-axis represents the markers including CD105, CD90, CD73 and nestin, one-way ANOVA. (R) Verification of the transcriptome results on the selected DEGs (RT-PCR, three individual wells/cell type) among AnPC, DPC and PPC, one-way ANOVA. \*\*\*\* $p < 0.0001$ , \*\*\* $p < 0.001$ , \*\* $p < 0.01$ , \* $p < 0.05$ .

PPC is significantly longer than that between DPC and PPC, suggesting AnPC separate from DPC and PPC evidently, while DPC and PPC showed few variations (Fig. 3A). This is consistent with the results from hierarchical clustering analysis on the same unigenes, with AnPC showing a distinguished gene expression profile whereas DPC and PPC clustering together as a composite group (Fig. 3B). The DEG analysis between DPC and PPC suggests only 18 DEGs existed between PPC and DPC (Fig. 3D), while 1475 DEGs existed between DPC and AnPC (Fig. 3E) and 1314 DEGs existed between PPC and AnPC (Fig. 3F,  $|\log_2\text{foldchange}| \geq 1$ , adjusted  $p$  value  $\leq 0.01$ ). Thus, the analysis results above suggest DPC and PPC maintained the same gene expression pattern, while AnPC demonstrated the distinctive gene expression.

To further analyze the different functions between PPSC and AnPC, we generated co-expressed 1270 DEGs (Co-PC) from 1475 DPC-AnPC DEGs and 1314 PPC-AnPC DEGs via Venn analysis ( $|\log_2\text{foldchange}| \geq 1$ , adjusted  $p$  value  $\leq 0.01$ , Fig. 3C). The results of biological process of GO analyses showed the up-regulated genes of AnPC compared to PPSC (Co-PC) were mainly classified into the categories of protein ubiquitination, Wnt signaling pathway, extracellular matrix organization, angiogenesis and neuron differentiation, etc. ( $p < 0.01$ , Fig. 4A). In view of a lot of GO terms relating to angiogenesis and neurodevelopment, the co-expressed genes were additionally summarized from all angiogenesis-relevant GO terms (Fig. 4D) and from all neurogenesis-relevant GO terms (Fig. 4E). The KEGG pathway analysis showed that the up-regulated genes of AnPC compared to Co-PC were mainly enriched in pathways in proteoglycans in cancer, axon guidance, vascular smooth muscle contraction, Hippo signaling pathway and cGMP-PKG signaling pathway, etc. ( $p \leq 0.05$ , Fig. 4C).

Different from AnPC, the up-regulated genes of PPSC were mainly enriched in biological process of GO terms related to intracellular signal transduction, mRNA splicing via spliceosome, transcription, intracellular protein transport and androgen receptor signaling pathway, etc. ( $p < 0.01$ , Fig. 4A). The highly enriched KEGG pathway networks in Co-PC mainly included PI3K-Akt signaling pathway, MAPK signaling pathway and insulin signaling pathway, etc. ( $p < 0.05$ , Fig. 4C). We additionally did the gene regulating network analysis using the 3007 co-expressed genes between DPC and PPC ( $|\log_2\text{foldchange}| < 1$ , gene expression  $\geq 100$ ) to specifically detect the functions of PPSC on antler regeneration. Similar to the above GO analysis of up-regulated genes of AnPC, most genes were enriched in RNA metabolic process, macromolecular metabolic process and regulation of signal transduction (Fig. 5), which are the typical characters of self-renew stem cells [53].

### 3.4 Real-time PCR analysis verified transcriptome results

Six DEGs between AnPC, DPC, and PPC (VEGFA, NR1P1, WNT5A, SOX11, USP34 and MACF1) were selected randomly to validate the transcriptome analysis result by RT-PCR (Fig. 2R). The results showed that the gene expression levels of the six genes were all significantly higher in AnPC than DPC and PPC ( $p \leq 0.01$ ), whereas no gene expression difference exists between DPC and PPC. The q-PCR results were consistent with the transcriptome results (Table 1).

## 4. Discussion

Pedicle periosteum and antler periosteum can both support antler regeneration. However, the regenerative capacity of the antler periosteum is much weaker than that of pedicle periosteum [10,11,18]. To detect the factors owing to this difference, we constructed the *in vitro* culture system for sika deer antler periosteum using the same culture condition as that for the pedicle stem cells. The isolated antler periosteal cells (AnPC) demonstrated same mesenchyme stem cell (MSC) markers as the pedicle periosteal stem cells (PPC and DPC). However, the fluorescence degree of the markers and the proliferation rate in AnPC were significantly decreased, compared to those of PPC and DPC. The proliferation rates of AnPC also decreased after successive passages. The overall findings may in part explain the weakened regenerative capacity of antler periosteum during antler regeneration. During the cell culture process, the stemness of AnPC, DPC and PPC were gradually increased as the mesospheres clustered from the monolayer cells by changing the culture medium from DMEM/FBS medium into serum-free MSC medium. Similar phenomenon was also observed in other MSC derived stem cell lineage, accompanied by the recovered regenerative ability [54]. The serum-free MSC medium has been proved to better preserve the function and multi-potentiality of the MSCs, compared to the medium containing FBS [55]. It would be interesting to compare the regenerative capacities of the monolayer periosteal cells to the periosteal mesospheres in the future study.

In view of the attenuated regenerative capacity of antler periosteum, we hypothesized that the antler periosteum and the pedicle periosteum maintained distinct functions during antler regeneration. Therefore, comparative transcriptional analysis was conducted on AnPC, PPC and DPC. We found that the up-regulated genes of AnPC mainly related to angiogenesis, neuron differentiation and osteoblastogenesis of MSC in intramembranous ossification, whereas the up-regulated genes of the pedicle periosteal stem cells were enriched in the relevant terms of stem cell renewal. Along with the fast growth of antler, the average growth rates of sika deer antler external tissues including blood vessels and nerves can reach up to 1.14 cm/day during antler fast-growth period [17]. Antlers are richly vascularized during growth. The antler arter-

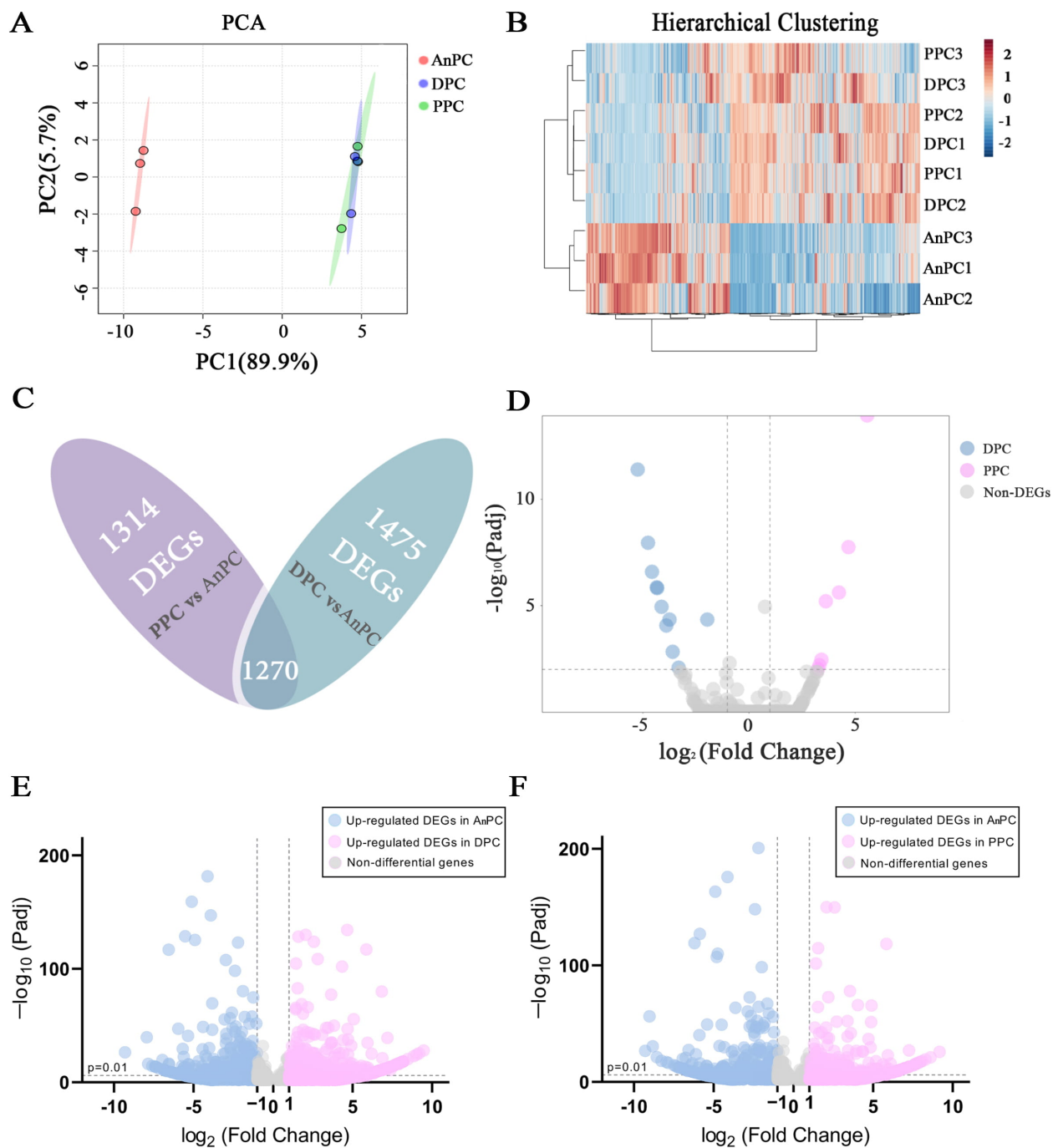


**Fig. 3. A general view of gene expression pattern and DEG analysis on AnPC, DPC and PPC.** (A) The PCA analysis performed on the transcript signatures of DPC, PPC and AnPC. (B) The hierarchical clustering analysis performed on the transcript signatures of AnPC, DPC and PPC. (C) Venn analysis performed to selected the co-expressed DEGs between the AnPC-PPC DEGs and AnPC-DPC DEGs. (D-F) Volcano plots showing the expression level of DEGs (D) between DPC and PPC, (E) between APC and DPC, and (F) between APC and PPC, respectively. X-axis represents the  $\log_2$ foldchange values of the DEGs. The values  $\geq 1$  and  $\leq -1$  are marked by grey color. The values  $\geq 1$  are marked by pink color, representing the up-regulated genes of PPC and the values  $\leq -1$  are marked by blue colors, representing the up-regulated genes of DPC. Y-axis denotes  $-\log_{10}$  value of adjusted  $p$  value (padj) of DEGs,  $\text{padj} \leq 0.01$ . DEGs, differentially expressed genes.

ies regenerate from the pedicle artery stumps, which originate from the branches of the superficial temporal artery [56]. They elongate within the loose connective tissue be-

tween dermis and antler periosteum (vascular layer) and extensively branch in tip area, as the arteries begin to curve around the tip of the antler. The arteries branched prox-

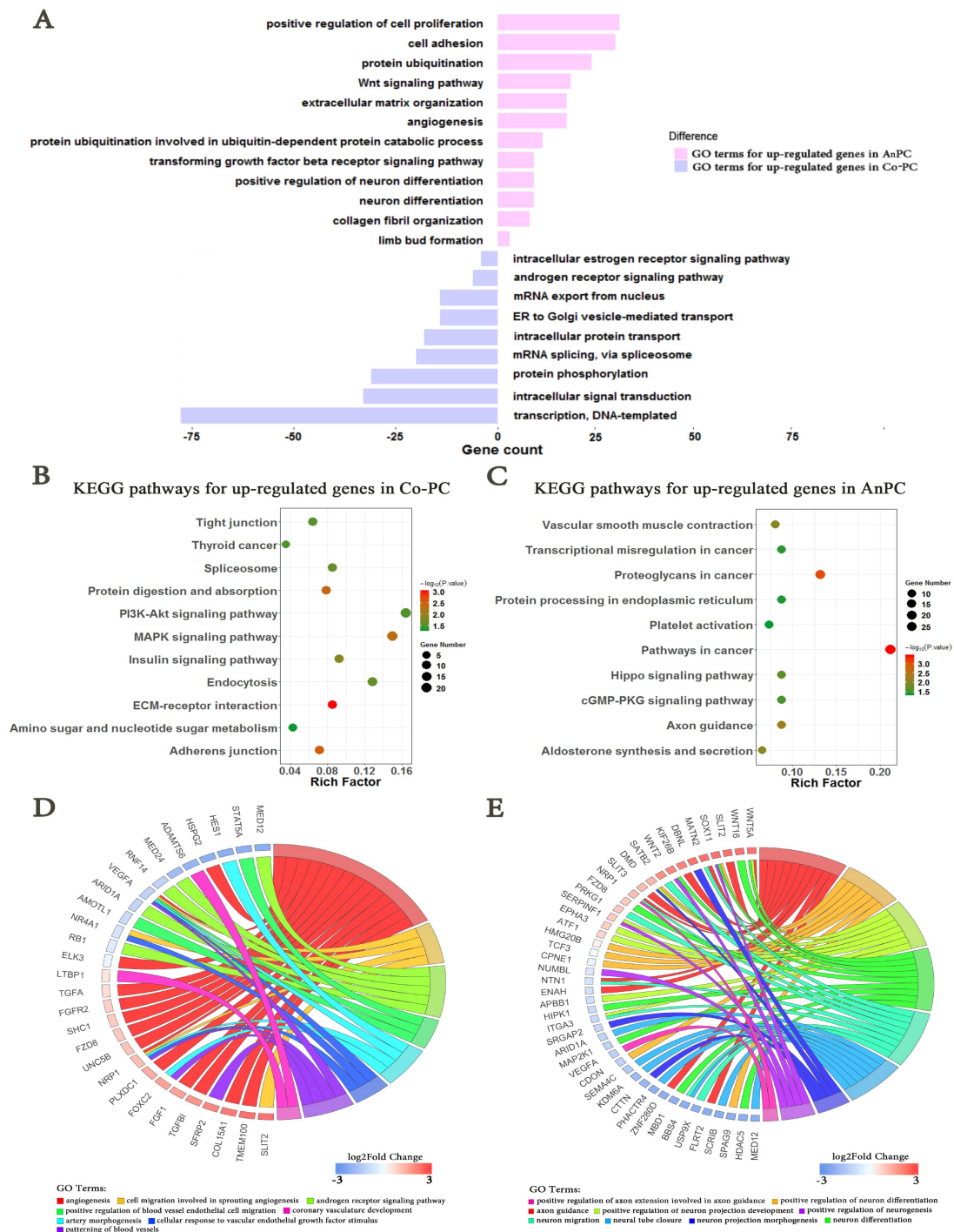


**Fig. 4. Gene functional analysis on DEGs between AnPC and Co-PC.** (A) GO analysis in BP performed on the 1270 DEGs between AnPC and Co-PC. The X-axis denotes the gene counts of the enriched GO terms. Y-axis represents the important GO terms ( $p \leq 0.01$ ). The pink bar represents the GO terms that up-regulated genes of AnPC enriched and the blue bar represents the GO terms that up-regulated genes of Co-PC enriched. (B, C) KEGG analysis performed on the (B) 544 up-regulated DEGs of Co-PC compared to AnPC and (C) on the 726 up-regulated DEGs of APC compared to Co-PC, respectively. The vertical axis represents the highest ranked KEGG terms according to the gene counts. The colors from red to green represent the  $-\log_{10}$  value of adjusted  $p$  values (adjusted  $p$  values  $\leq 0.01$ ). The horizontal axis represents gene ratio, which is the percentage of total DEGs in the given GO term. (D–E) Enriched DEGs relating to GO terms on (D) angiogenesis and (E) neurodevelopment, respectively. The colors from red to blue represent  $\log_2$ foldchange values of the DEGs. GO, gene ontology; BP, biological process; DEG, differentially expressed gene; Gene counts, the number of genes enriched in a GO term, represented by the different sizes of the circles; Co-PC, co-expressed DEGs between AnPC-DPC DEGs and AnPC-PPC DEGs.

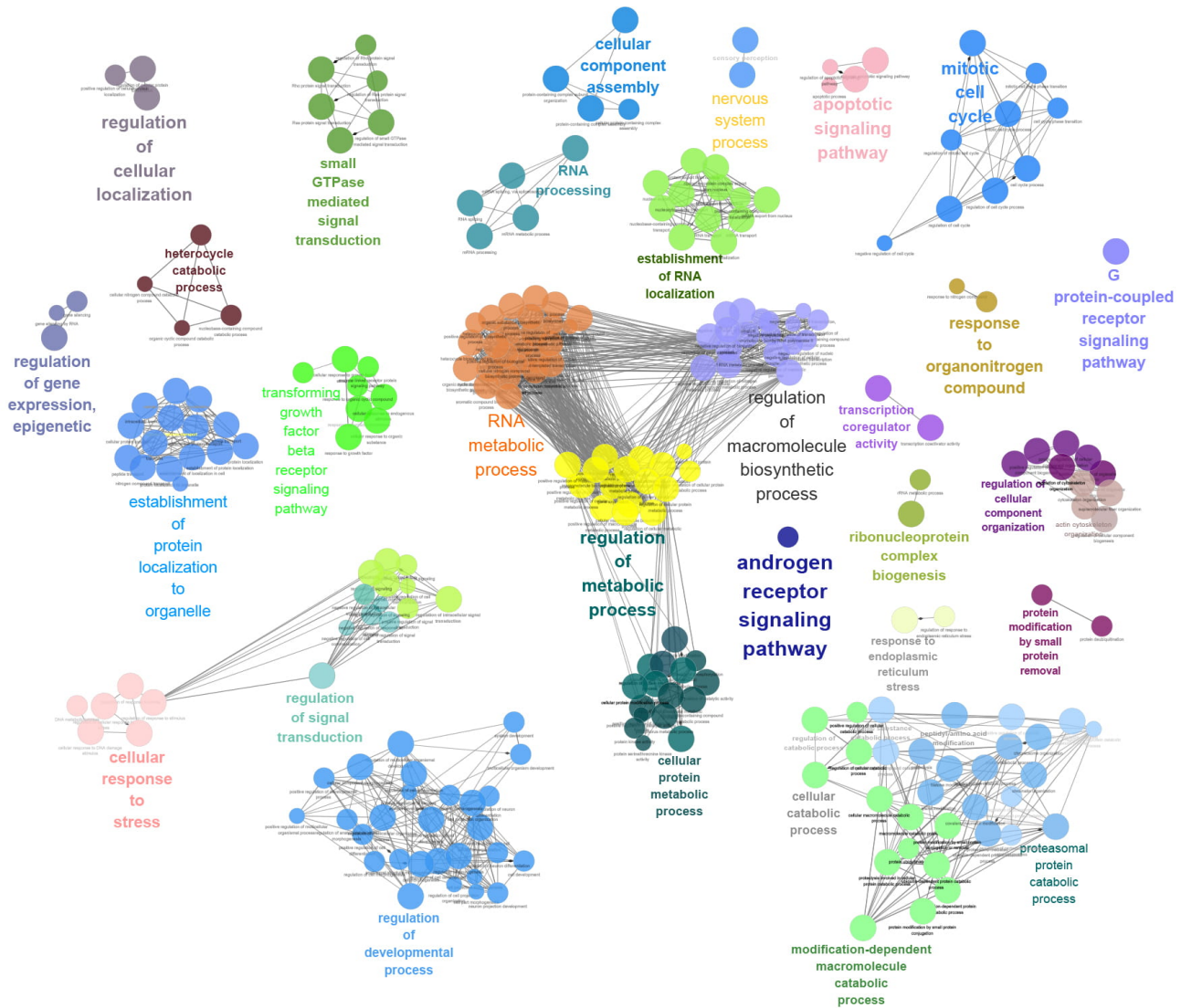


**Fig. 5. Gene regulating network analysis on the 5036 co-expressed genes between PPC and DPC.** The nodes from the network label the biological process of GO terms, which are linked based on a pre-defined kappa score level. The nodes with similar functions are merged into distinguished functional group based on the predefined kappa score threshold (0–1), paired in the same color. The functional groups represented by their most significant term are selected manually and visualized in the network by bigger font. The size of the nodes reflects the enrichment significance of the terms. DPC, the stem cells cultured from proximal two-thirds of the pedicle periosteal; PPC, the stem cells cultured from the distal third of periosteal.

imally into the hyperplastic perichondrium to give rise to the ordered parallel array of venous vessels running distal to proximal into the pre-cartilage layer, cartilage layer and bone as the antler elongates [57]. Blood flows into the antler from the arteries distally to proximally and returns via the venous vessels [56,57]. The significant vascular extension of antler mainly happens in the antler arteries within vascular layer and in the branching venous vessels within the pre-cartilage layer [57]. Morphologically, the arteries of a growing antler are very close to antler periosteum [58].

On transcriptional level, our study detected AnPC expressed large abundance of angiogenesis promoting genes, including VEGFA, NRP1, FOXC2, TGF- $\beta$ , FGF1, LTBP-

1, SLIT2 and STAT5A, etc. The vascular endothelial growth factors (VEGFs) are well known as central regulators of pro-angiogenic activity [59,60]. Among them, VEGFA is a key angiogenic factor, which regulate embryonic arterial differentiation and branching [61]. In adult vascular development, VEGF-A regulates most aspects of the endothelial response, such as the proliferation and migration of endothelial cells, vascular permeability and induction of tip cell migration and stalk cell proliferation [62]. In injury induced organ regeneration, VEGF-A regulates organ homeostasis through the release of paracrine factors from endothelial cells to promote organ regeneration [63]. Neuropilin 1 (NRP1) is a transmembrane glycoprotein be-

**Table 1. The 6 DEGs<sup>†</sup> between AnPC and Co-PC<sup>‡</sup>, including 6 up-regulated genes of AnPC ( $|\log_2\text{foldchange}| \geq 1$ , adjusted  $p$  value  $\leq 0.01$ ).**

Gene ID	Gene name	Gene symbol	Log2foldchange	Log2foldchange
			AnPC vs DPC	AnPC vs PPC
CL1721.Contig1_All	Microtubule Actin Crosslinking Factor 1	MACF1	1.67	1.79
Unigene50452_All	Neuropilin 1	NRP1	1.57	1.52
CL4251.Contig1_All	Wnt Family Member 5A	WNT5A	5.62	6.75
CL140.Contig10_All	Ubiquitin Specific Peptidase 34	USP34	1.63	1.66
CL3165.Contig2_All	Vascular Endothelial Growth Factor A	VEGFA	1.50	1.61
Unigene22604_All	SRY-Box Transcription Factor 11	SOX11	4.30	4.95

<sup>†</sup>DEGs, differentially expressed genes; <sup>‡</sup>Co-PC, co-expressed DEGs from DPC-AnPC DEGs and PPC-AnPC DEGs.

longing to the neuropilin family, which is an essential modulator of embryonic angiogenesis, vessel remodeling and adult arteriogenesis [64–66]. The Forkhead/Fox transcription factor (FOXO2) is another critical regulator of vascular development [67], required for the formation of the aortic arch and arterial-venous specification during embryonic development [68,69]. It also promotes endothelial cell migration and microvessel formation *in vitro* [70]. Transforming growth factor- $\beta$  (TGF- $\beta$ ) is a cell growth factor, regulating the differentiation of vascular smooth muscle cells [71] and promoting the pro-angiogenesis [72,73]. FGF1 belongs to the FGF family, which exerts the pro-angiogenic effect [74,75] and increases the number of blood vessels [76]. FGF1 and VEGF-A can also be synergistic to stimulate a greater angiogenic response [77]. Latent TGF-beta binding protein 1 (LTBP-1) [78] and slit protein 2 (SLIT2) [79] both function on vascular remodeling. The transcription factors signal transducer and activator of transcription 5A (STAT5A) are required for hematopoietic stem cell maintenance and self-renewal [80]. Overall, our results suggested AnPC may function as a niche for antler angiogenesis, contributing to the artery fast growth, vascular wall development and homeostasis during antler regeneration.

Growing antlers are profusely innervated by solely sensory fibers regenerating from the pedicle sensory nerve stumps, which are derived from the zygomaticotemporal and supraorbital branches of the trigeminal nerve [81–84]. The newly regenerative antler nerves also elongate within the vascular layer peripherally, following very closely the distribution of antler arteries [11,81,83,85]. The profuse nerve fibers occur in small bundles, projecting from the vascular layer towards more superficial layers of the velvet skin [27,83]. In antler tip, the nerve fibers follow the route of the artery branches, abundantly locating at the deep connective tissue above the reserve mesenchyme of the antler [83,86,87]. The nerve fibers also distribute in subepidermis, perichondrium, but only sparse fibers are seen in the pre-cartilage layer [86,87]. The antler nerve consists of both myelinated and nonmyelinated fibers [81–83], with known function as perceiving the environmental stimulus [83,86] and determining antler size and shape [11,81]. Den-

ervation of the antler does not affect their regenerative capacity, but the regenerative antlers are significantly smaller and of changed shape. Previous studies identified some of the axon growth promoters that were secreted by arterial smooth muscle [87], pedicle periosteum [58] and velvet skin [88–90]. In this study, we found AnPC expressed more neurogenesis promoting genes for the first time, including WNT5A, WNT2, SOX11, MATN2, BBS4 and NTN1, etc. Wnts are a family of secreted, lipidated proteins regulating the self-renewal, maintenance, and differentiation of neural progenitor cells during embryonic and adult development of the nervous system [91–94]. Regarding the Wnt ligands, WNT5A is one of the critical noncanonical endogenous ligands that promote neuronal differentiation of progenitor cells and the neurogenesis as a niche factor during cerebellum [95], cerebral cortex, midbrain [96–98] and hippocampus development [95,99,100]. WNT2 increases dopaminergic progenitor proliferation and neuron development [101]. It also participates in synapse development [102]. The transcription factor Sox11 is another important factor on nervous system development and regenerative transcriptional control program. Sox11 is particularly expressed at high levels in sensory neurons [103–105], promoting the neuron survival and neurite outgrowth. *In vitro* culture, Sox11 is also necessary for survival and axonal growth of adult sensory neurons [104]. In addition, Sox11 contributes to retinal ganglion neuronal survival and axon regeneration [106,107] and peripheral nerve regeneration [105]. Matrilin 2 (MATN2) encodes the adaptor protein of the extracellular matrix, expressed by pre-myelinating Schwann cells during normal development. MATN2 increase neurite outgrowth of dorsal root ganglia neurons and enhances the migration of dorsal root ganglia derived Schwann cells. When peripheral nerves are injured, MATN2 contributes to axon regeneration through promoting axonal growth and cell migration [108]. BBS4 encodes Bardet-Biedl syndrome protein 4 that mainly localizes in the cilium of oligodendrocytes of central nerve system and neurosensory organs [109]. It functions as maintaining the length and quantity of sensory neuron cilium [110]. Netrin 1 (NTN1) is a secreted molecule of the laminin superfamily [111] that is best known for its

role in axon guidance [112] and neuronal survival [113]. In this study, the large amount of up-regulated genes relating to neurogenesis strongly demonstrated the important function of the AnPC on promoting nerve regeneration and fast growth.

In addition, up-regulated genes of AnPC were also enriched in Wnt signaling pathway. This finding is consistent with a previous study, showing that the activated  $\beta$ -catenin was localized in the antler periosteum and the osteoblasts were lined with the newly formed bone during antler rapid-growth period [114]. Our study identified more Wnt pathway relevant genes from antler periosteum, including USP34, MACF1 and WNT16. The ubiquitin-specific protease 34 (USP34) is an essential regulator of osteogenesis, which contributes to bone formation by promoting the osteogenic differentiation of MSC while inhibiting osteoclast differentiation [115]. Conditional knockout of USP34 leads to low bone mass and impaired bone regeneration [116]. Microtubule actin crosslinking factor 1 (MACF1) is another important gene that promotes the osteogenic differentiation of MSC [117]. MACF1 encodes MACF1 spectraplaklin protein, which can initiate the osteogenic pathways and up-regulate osteoblast proliferation through enhancing  $\beta$ -catenin signaling and preosteoblast migration [118]. Loss of MACF1 attenuates the osteogenic potential of MSC and impairs bone properties and bone strength [117,119]. The WNT16 influences bone mineral density, cortical bone thickness and bone strength through inhibiting human and mouse osteoclastogenesis [120]. The deletion of WNT16 leads to spontaneous fractures as a result of low cortical thickness and high cortical porosity [121]. The latitudinal growth of the antler is via intramembranous ossification by the osteoblasts derived from the antler periosteum [25–27,31]. The Wnt pathway enriched genes detected in AnPC may function as increasing bone mass and promoting the osteoblastogenesis of MSC in intramembranous ossification so that to support the fast growth of the antler without osteoporosis.

In conclusion, we show cultured antler periosteal cells (AnPC) expressed weaker MSC markers and lower cell proliferative potential than pedicle periosteal stem cells (PPSC). These findings may partly explain the weakened regenerative capacity of the antler periosteum, compared to the pedicle periosteum. From comparing the gene expression profiles of AnPC with those of PPSC, we suggest that the AnPC may function as promoting antler fast growth through contributing to the angiogenesis, neurogenesis and intramembranous ossification. Our study will help better understand the important role of antler periosteum during antler regeneration. The selected genes relating to promoting angiogenesis, neurogenesis and intramembranous ossification may be of essential value on the clinical applications in the future.

## Author contributions

HS and GW designed the research study. GW, XL, ZW, YW, QG, WS, and LX performed the research. HS provided help and advice on sample extraction and cell culture. TQ and GW analyzed the data. GW wrote the manuscript. SZ provided manuscript review and editing. All authors contributed to editorial changes in the manuscript. All authors read and approved the final manuscript.

## Ethics approval and consent to participate

The protocol and procedures employed in this study were ethically reviewed and approved according to the Animal Ethics Committee of the Institute of Special Wild Economic Animals and Plants, Chinese Academy of Agricultural Sciences (Permit Number: CAAS2017046C, approved since 22 March 2017).

## Acknowledgment

We thank C. Li for his supports for this study.

## Funding

This research was funded by the Jilin Province Science and Technology Development Plan Project, grant number 20190201292JC.

## Conflict of interest

The authors declare no conflict of interest.

## Supplementary material

Supplementary material associated with this article can be found, in the online version, at <https://www.imrpress.com/journal/FBL/27/2/10.31083/j.fbl2702069>.

## References

- [1] Chang H, Knothe Tate ML. Concise review: the periosteum: tapping into a reservoir of clinically useful progenitor cells. *Stem Cells Translational Medicine*. 2014; 1: 480–491.
- [2] Colnot C. Skeletal cell fate decisions within periosteum and bone marrow during bone regeneration. *Journal of Bone and Mineral Research*. 2009; 24: 274–282.
- [3] Colnot C, Zhang X, Tate MLK. Current insights on the regenerative potential of the periosteum: Molecular, cellular, and endogenous engineering approaches. *Journal of Orthopaedic Research*. 2012; 30: 1869–1878.
- [4] Ferretti C, Mattioli-Belmonte M. Periosteum derived stem cells for regenerative medicine proposals: Boosting current knowledge. *World Journal of Stem Cells*. 2014; 6: 266–277.
- [5] van Gastel N, Torrekens S, Roberts SJ, Moermans K, Schrooten J, Carmeliet P, *et al.* Engineering Vascularized Bone: Osteogenic and Proangiogenic Potential of Murine Periosteal Cells. *Stem Cells*. 2012; 30: 2460–2471.
- [6] Roberts SJ, van Gastel N, Carmeliet G, Luyten FP. Uncovering the periosteum for skeletal regeneration: the stem cell that lies beneath. *Bone*. 2015; 70: 10–18.
- [7] Thabet AM, Paley D, Kocaoglu M, Eralp L, Herzenberg JE, Ergin ON. Periosteal grafting for congenital pseudarthrosis of the

- tibia: a preliminary report. *Clinical Orthopaedics and Related Research*. 2008; 466: 2981–2994.
- [8] Zhang X, Xie C, Lin ASP, Ito H, Awad H, Lieberman JR, *et al*. Periosteal progenitor cell fate in segmental cortical bone graft transplantations: implications for functional tissue engineering. *Journal of Bone and Mineral Research*. 2005; 20: 2124–2137.
- [9] Li C, Mackintosh CG, Martin SK, Clark DE. Identification of key tissue type for antler regeneration through pedicle periosteum deletion. *Cell and Tissue Research*. 2007; 328: 65–75.
- [10] GOSS RJ. Experimental investigation of morphogenesis in the growing antler. *Journal of Embryology and Experimental Morphology*. 1961; 9: 342–354.
- [11] Suttie JM, Fennessy PF. Regrowth of amputated velvet antlers with and without innervation. *The Journal of Experimental Zoology*. 1985; 234: 359–366.
- [12] Fennessy PF, Suttie JM. Antler growth: Nutritional and endocrine factors. *Biology of Deer Production*, New Zealand, Royal Soc New Zealand. 1985; 22: 239–250.
- [13] Li C, Clark DE, Suttie JM. Deer pedicle height, tissue interactions and antler evolution. *Deer*. 2003; 12: 333–338.
- [14] Goss RJ. Inhibition of growth and shedding of antlers by sex hormones. *Nature*. 1968; 220: 83–85.
- [15] Bartoš L, Schams D, Bubenik GA. Testosterone, but not IGF-1, LH, prolactin or cortisol, may serve as antler-stimulating hormone in red deer stags (*Cervus elaphus*). *Bone*. 2009; 44: 691–698.
- [16] Goss RJ. *Deer Antler: Regeneration, Function and Evolution*. Academic Press: New York. 1983.
- [17] Gao ZG, Li C, Liu ZA, Du YC. Study on the relationship between growth rate, ossification degree and testosterone, estradiol and alkaline phosphatase of sika deer antler. *Acta Veterinaria et Zootechnica Sinica*. 1988; 19: 171–176.
- [18] Li C. Residual antler periosteum holds the potential to partially regenerate lost antler tissue. *Journal of Experimental Zoology Part A: Ecological and Integrative Physiology*. 2021; 335: 386–395.
- [19] Li C, Suttie JM, Clark DE. Morphological observation of antler regeneration in red deer (*Cervus elaphus*). *Journal of Morphology*. 2004; 262: 731–740.
- [20] Allen MR, Hock JM, Burr DB. Periosteum: biology, regulation, and response to osteoporosis therapies. *Bone*. 2004; 35: 1003–1012.
- [21] Duchamp de Lageneste O, Julien A, Abou-Khalil R, Frangi G, Carvalho C, Cagnard N, *et al*. Periosteum contains skeletal stem cells with high bone regenerative potential controlled by Periostin. *Nature Communications*. 2018; 9: 773.
- [22] Li C, Yang F, Sheppard A. Adult stem cells and mammalian epimorphic regeneration—insights from studying annual renewal of deer antlers. *Current Stem Cell Research & Therapy*. 2009; 4: 237–251.
- [23] Wang D, Berg D, Ba H, Sun H, Wang Z, Li C. Deer antler stem cells are a novel type of cells that sustain full regeneration of a mammalian organ—deer antler. *Cell Death & Disease*. 2019; 10: 443.
- [24] Ker DFE, Wang D, Sharma R, Zhang B, Passarelli B, Neff N, *et al*. Identifying deer antler uhrf1 proliferation and s100a10 mineralization genes using comparative RNA-seq. *Stem Cell Research & Therapy*. 2018; 9: 292.
- [25] Kierdorf U, Stoffels E, Stoffels D, Kierdorf H, Szuwart T, Clemen G. Histological studies of bone formation during pedicle restoration and early antler regeneration in roe deer and fallow deer. *The Anatomical Record Part A, Discoveries in Molecular, Cellular, and Evolutionary Biology*. 2003; 273: 741–751.
- [26] Li C, Suttie JM. Light microscopic studies of pedicle and early first antler development in red deer (*Cervus elaphus*). *The Anatomical Record*. 1994; 239: 198–215.
- [27] Li C, Suttie JM, Clark DE. Histological examination of antler regeneration in red deer (*Cervus elaphus*). *The Anatomical Record Part A, Discoveries in Molecular, Cellular, and Evolutionary Biology*. 2005; 282: 163–174.
- [28] Price J, Allen S. Exploring the mechanisms regulating regeneration of deer antlers. *Philosophical Transactions of the Royal Society of London. Series B, Biological Sciences*. 2004; 359: 809–822.
- [29] Price JS, Allen S, Fauchaux C, Althnaian T, Mount JG. Deer antlers: a zoological curiosity or the key to understanding organ regeneration in mammals? *Journal of Anatomy*. 2005; 207: 603–618.
- [30] Dong Z, Haines S, Coates D. Proteomic Profiling of Stem Cell Tissues during Regeneration of Deer Antler: a Model of Mammalian Organ Regeneration. *Journal of Proteome Research*. 2020; 19: 1760–1775.
- [31] Li C, Clark DE, Lord EA, Stanton JL, Suttie JM. Sampling technique to discriminate the different tissue layers of growing antler tips for gene discovery. *The Anatomical Record*. 2002; 268: 125–130.
- [32] Banks JW, Newbrey WJ. Antler development as a unique modification of mammalian endochondral ossification. Antler development in Cervidae. TX Cesar Kleburg Wildlife Research Institute. Kingsville. 1983; 279–306.
- [33] Goss RJ. Problems of antlerogenesis. *Clinical Orthopaedics and Related Research*. 1970; 69: 227–238.
- [34] Tsai A, Stamoulis C, Barber I, Kleinman PK. Infant lower extremity long bone growth rates: comparison of contemporary with early 20th century data using mixed effect models. *American Journal of Human Biology*. 2017; 29.
- [35] Ha JH, Choi IH, Chung CY, Cho TJ, Jung ST, Lee HS, *et al*. Distribution of Lengths of the Normal Femur and Tibia in Korean Children from Three to Sixteen Years of Age. *Journal of Korean Medical Science*. 2003; 18: 715–721.
- [36] Pritchett JW. Longitudinal growth and growth-plate activity in the lower extremity. *Clinical Orthopaedics and Related Research*. 1992; 274–279.
- [37] Li C, Suttie JM. Tissue collection methods for antler research. *European Journal of Morphology*. 2003; 41: 23–30.
- [38] Li C, Littlejohn RP, Suttie JM. Effects of insulin-like growth factor 1 and testosterone on the proliferation of antlerogenic cells *in vitro*. *The Journal of Experimental Zoology*. 1999; 284: 82–90.
- [39] Grabherr MG, Haas BJ, Yassour M, Levin JZ, Thompson DA, Amit I, *et al*. Full-length transcriptome assembly from RNA-Seq data without a reference genome. *Nature Biotechnology*. 2011; 29: 644–652.
- [40] Altschul SF, Gish W, Miller W, Myers EW, Lipman DJ. Basic local alignment search tool. *J Mol Biol*. 1990; 215(3):403–410. doi:10.1016/S0022-2836(05)80360-2
- [41] Langmead B, Salzberg S. Fast gapped-read alignment with Bowtie 2. *Nature Methods*. 2012; 9:357–359.
- [42] Li B, Dewey CN. RSEM: accurate transcript quantification from RNA-Seq data with or without a reference genome[J]. *BMC Bioinformatics*, 2011, 12: 323.
- [43] Chong J, Soufan O, Li C, Caraus I, Li S, Bourque G, *et al*. MetaboAnalyst 4.0: towards more transparent and integrative metabolomics analysis. *Nucleic Acids Research*. 2018; 46: W486–W494.
- [44] Anders S, Huber W. Differential expression analysis for sequence count data. *Genome Biology*. 2010; 11: R106.
- [45] Huang DW, Sherman BT, Lempicki RA. Systematic and integrative analysis of large gene lists using DAVID bioinformatics resources. *Nature Protocols*. 2009; 4: 44–57.
- [46] Shannon P, Markiel A, Ozier O, Baliga NS, Wang JT, Ramage D, *et al*. Cytoscape: a software environment for integrated models of biomolecular interaction networks. *Genome Research*. 2003;

- 13: 2498–2504.
- [47] Widera D, Zander C, Heidbreder M, Kasperek Y, Noll T, Seitz O, *et al.* Adult Palatum as a Novel Source of Neural Crest-Related Stem Cells. *Stem Cells*. 2009; 27: 1899–1910.
- [48] Shi H, Zhang T, Qiang L, Man L, Shen Y, Ding F. Mesenspheres of neural crest-derived cells enriched from bone marrow stromal cell subpopulation. *Neuroscience Letters*. 2013; 532: 70–75.
- [49] Méndez-Ferrer S, Michurina TV, Ferraro F, Mazloom AR, Macarthur BD, Lira SA, *et al.* Mesenchymal and haematopoietic stem cells form a unique bone marrow niche. *Nature*. 2010; 466: 829–834.
- [50] Sviderskaya EV, Easty DJ, Lawrence MA, Sánchez DP, Negulyaev YA, Patel RH, *et al.* Functional neurons and melanocytes induced from immortal lines of postnatal neural crest-like stem cells. *FASEB Journal*. 2009; 23: 3179–3192.
- [51] Fernandes KJL, McKenzie IA, Mill P, Smith KM, Akhavan M, Barnabé-Heider F, *et al.* A dermal niche for multipotent adult skin-derived precursor cells. *Nature Cell Biology*. 2004; 6: 1082–1093.
- [52] Molofsky AV, Pardal R, Iwashita T, Park I, Clarke MF, Morrison SJ. Bmi-1 dependence distinguishes neural stem cell self-renewal from progenitor proliferation. *Nature*. 2003; 425: 962–967.
- [53] Ito K, Suda T. Metabolic requirements for the maintenance of self-renewing stem cells. *Nature Reviews Molecular Cell Biology*. 2014; 15: 243–256.
- [54] Wei G, Sun H, Wei H, Qin T, Yang Y, Xu X, *et al.* Detecting the Mechanism behind the Transition from Fixed Two-Dimensional Patterned Sika Deer (*Cervus nippon*) Dermal Papilla Cells to Three-Dimensional Pattern. *International Journal of Molecular Sciences*. 2021; 22: 4715.
- [55] Meuleman N, Tondreau T, Delforge A, Dejeneffe M, Massy M, Libertalis M, *et al.* Human marrow mesenchymal stem cell culture: serum-free medium allows better expansion than classical alpha-MEM medium. *European Journal of Haematology*. 2006; 76: 309–316.
- [56] Suttie JM, Fennessy PF, Mackintosh CG, Corson ID, Christie R, Heap SW. Sequential cranial angiography of young deer stags. *Biology of Deer Production*. Fennessy PF, Drew K (eds). R Soc NZ Wellington Bull. 1985a; 22: 263–268.
- [57] Clark DE, Li C, Wang W, Martin SK, Suttie JM. Vascular localization and proliferation in the growing tip of the deer antler. *the Anatomical Record. Part A, Discoveries in Molecular, Cellular, and Evolutionary Biology*. 2006; 288: 973–981.
- [58] Li C. Deer antler regeneration: a stem cell-based epimorphic process. *Birth Defects Research. Part C, Embryo Today*. 2012; 96: 51–62.
- [59] Melnicovici CS, Boşca AB, Şuşman S, Mărginean M, Mişu C, Istrate M, *et al.* Vascular endothelial growth factor (VEGF) - key factor in normal and pathological angiogenesis. *Romanian Journal of Morphology and Embryology*. 2018; 59: 455–467.
- [60] Coultas L, Chawengsaksophak K, Rossant J. Endothelial cells and VEGF in vascular development. *Nature*. 2005; 438: 937–945.
- [61] Li W, Kohara H, Uchida Y, James JM, Soneji K, Cronshaw DG, *et al.* Peripheral nerve-derived CXCL12 and VEGF-A regulate the patterning of arterial vessel branching in developing limb skin. *Developmental Cell*. 2013; 24: 359–371.
- [62] Blanco R, Gerhardt H. VEGF and Notch in tip and stalk cell selection. *Cold Spring Harbor Perspectives in Medicine*. 2013; 3: a006569.
- [63] Ding B, Nolan DJ, Butler JM, James D, Babazadeh AO, Rosenwaks Z, *et al.* Inductive angiocrine signals from sinusoidal endothelium are required for liver regeneration. *Nature*. 2010; 468: 310–315.
- [64] Fantin A, Herzog B, Mahmoud M, Yamaji M, Plein A, Denti L, *et al.* Neuropilin 1 (NRP1) hypomorphism combined with defective VEGF-A binding reveals novel roles for NRP1 in developmental and pathological angiogenesis. *Development*. 2014; 141: 556–562.
- [65] Plein A, Fantin A, Ruhrberg C. Neuropilin regulation of angiogenesis, arteriogenesis, and vascular permeability. *Microcirculation*. 2014; 21: 315–323.
- [66] Lanahan A, Zhang X, Fantin A, Zhuang Z, Rivera-Molina F, Speichinger K, *et al.* The neuropilin 1 cytoplasmic domain is required for VEGF-a-dependent arteriogenesis. *Developmental Cell*. 2013; 25: 156–168.
- [67] Kume T. Foxc2 Transcription Factor: a Newly Described Regulator of Angiogenesis. *Trends in Cardiovascular Medicine*. 2008; 18: 224–228.
- [68] Kume T, Jiang H, Topczewska JM, Hogan BL. The murine winged helix transcription factors, Foxc1 and Foxc2, are both required for cardiovascular development and somitogenesis. *Genes & Development*. 2001; 15: 2470–2482.
- [69] Seo S, Fujita H, Nakano A, Kang M, Duarte A, Kume T. The forkhead transcription factors, Foxc1 and Foxc2, are required for arterial specification and lymphatic sprouting during vascular development. *Developmental Biology*. 2006; 294: 458–470.
- [70] Hayashi H, Sano H, Seo S, Kume T. The Foxc2 transcription factor regulates angiogenesis via induction of integrin beta3 expression. *The Journal of Biological Chemistry*. 2008; 283: 23791–23800.
- [71] Shi X, Guo L, Seedial SM, Si Y, Wang B, Takayama T, *et al.* TGF- $\beta$ /Smad3 inhibit vascular smooth muscle cell apoptosis through an autocrine signaling mechanism involving VEGF-a. *Cell Death & Disease*. 2015; 5: e1317.
- [72] Wang X, Abraham S, McKenzie JAG, Jeffs N, Swire M, Tripathi VB, *et al.* LRG1 promotes angiogenesis by modulating endothelial TGF- $\beta$  signalling. *Nature*. 2013; 499: 306–311.
- [73] Muppala S, Xiao R, Krukovets I, Verbovetsky D, Yendamuri R, Habib N, *et al.* Thrombospondin-4 mediates TGF- $\beta$ -induced angiogenesis. *Oncogene*. 2017; 36: 5189–5198.
- [74] Mori S, Tran V, Nishikawa K, Kaneda T, Hamada Y, Kawaguchi N, *et al.* A dominant-negative FGF1 mutant (the R50E mutant) suppresses tumorigenesis and angiogenesis. *PLoS ONE*. 2013; 8: e57927.
- [75] Guan JT, Li XX, Peng DW, Zhang WM, Qu J, Lu F, *et al.* MicroRNA-18a-5p Administration Suppresses Retinal Neovascularization by Targeting FGF1 and HIF1A. *Frontiers in Pharmacology*. 2020; 11: 276.
- [76] Husseman J, Palacios SD, Rivkin AZ, Oehl H, Ryan AF. The role of vascular endothelial growth factors and fibroblast growth factors in angiogenesis during otitis media. *Audiology & Neuro-Otology*. 2012; 17: 148–154.
- [77] Xue L, Greisler HP. Angiogenic effect of fibroblast growth factor-1 and vascular endothelial growth factor and their synergism in a novel *in vitro* quantitative fibrin-based 3-dimensional angiogenesis system. *Surgery*. 2002; 132: 259–267.
- [78] Saharinen J, Hyytiäinen M, Taipale J, Keski-Oja J. Latent transforming growth factor-beta binding proteins (LTBPs)—structural extracellular matrix proteins for targeting TGF-beta action. *Cytokine & Growth Factor Reviews*. 1999; 10: 99–117.
- [79] Dunaway CM, Hwang Y, Lindsley CW, Cook RS, Wu JY, Boothby M, *et al.* Cooperative signaling between Slit2 and Ephrin-A1 regulates a balance between angiogenesis and angiostasis. *Molecular and Cellular Biology*. 2011; 31: 404–416.
- [80] Maurer B, Kollmann S, Pickem J, Hoelbl-Kovacic A, Sexl V. STAT5A and STAT5B-Twins with Different Personalities in Hematopoiesis and Leukemia. *Cancers*. 2019; 11: 1726.
- [81] Wislocki GB, Singer M. The occurrence and function of nerves in the growing antlers of deer. *The Journal of Comparative Neurology*. 1946; 85: 1–19.

- [82] Adams JL. Innervation and blood supply of the antler pedicle of the Red deer. *New Zealand Veterinary Journal*. 1979; 27: 200–201.
- [83] Nieto-Diaz M, Pita-Thomas DW, Munoz-Galdeano T, Martinez-Maza C, Navarro-Ruiz R, Reigada D, *et al.* Deer antler innervation and regeneration. *Frontiers in Bioscience (Landmark Edition)*. 2012; 17: 1389–1401.
- [84] Woodbury MR, Haigh JC. Innervation and anesthesia of the antler pedicle in wapiti and fallow deer. *The Canadian Veterinary Journal*. 1996; 37: 486–489.
- [85] Vacek Z. Innervace lyci rostoucia parohu u cervidu. *Ceskoslovenska Morfologie*. 1955; 3: 249–264.
- [86] Gray C, Hukkanen M, Kontinen YT, Terenghi G, Arnett TR, Jones SJ, *et al.* Rapid neural growth: calcitonin gene-related peptide and substance P-containing nerves attain exceptional growth rates in regenerating deer antler. *Neuroscience*. 1992; 50: 953–963.
- [87] Li C, Stanton JL, Robertson TM, Suttie JM, Sheard PW, Harris AJ, *et al.* Nerve growth factor mRNA expression in the regenerating antler tip of red deer (*Cervus elaphus*). *PLoS ONE*. 2007; 2: e148.
- [88] Pita-Thomas W, Nieto-Sampedro M, Maza RM, Nieto-Diaz M. Factors promoting neurite outgrowth during deer antler regeneration. *Journal of Neuroscience Research*. 2010; 88: 3034–3047.
- [89] Pita-Thomas W, Barroso-García G, Moral V, Hackett AR, Cavalli V, Nieto-Diaz M. Identification of axon growth promoters in the secretome of the deer antler velvet. *Neuroscience*. 2017; 340: 333–344.
- [90] Pita-Thomas W, Fernández-Martos C, Yunta M, Maza RM, Navarro-Ruiz R, Lopez-Rodríguez MJ, *et al.* Gene expression of axon growth promoting factors in the deer antler. *PLoS ONE*. 2010; 5: e15706.
- [91] Hirabayashi Y, Itoh Y, Tabata H, Nakajima K, Akiyama T, Masuyama N, *et al.* The Wnt/beta-catenin pathway directs neuronal differentiation of cortical neural precursor cells. *Development*. 2004; 131: 2791–2801.
- [92] Munji RN, Choe Y, Li G, Siegenthaler JA, Pleasure SJ. Wnt signaling regulates neuronal differentiation of cortical intermediate progenitors. *The Journal of Neuroscience*. 2011; 31: 1676–1687.
- [93] Lie D, Colamarino SA, Song H, Désiré L, Mira H, Consiglio A, *et al.* Wnt signalling regulates adult hippocampal neurogenesis. *Nature*. 2005; 437: 1370–1375.
- [94] Zhang L, Yang X, Yang S, Zhang J. The Wnt/ $\beta$ -catenin signaling pathway in the adult neurogenesis. *The European Journal of Neuroscience*. 2011; 33: 1–8.
- [95] Subashini C, Dhanesh SB, Chen C, Riya PA, Meera V, Divya TS, *et al.* Wnt5a is a crucial regulator of neurogenesis during cerebellum development. *Scientific Reports*. 2017; 7: 42523.
- [96] Pino D, Choe Y, Pleasure SJ. Wnt5a controls neurite development in olfactory bulb interneurons. *ASN Neuro*. 2011; 3: e00059.
- [97] Andersson ER, Salto C, Villaescusa JC, Cajanek L, Yang S, Bryjova L, *et al.* Wnt5a cooperates with canonical Wnts to generate midbrain dopaminergic neurons in vivo and in stem cells. *Proceedings of the National Academy of Sciences*. 2013; 110: E602–E610.
- [98] Endo M, Doi R, Nishita M, Minami Y. Ror family receptor tyrosine kinases regulate the maintenance of neural progenitor cells in the developing neocortex. *Journal of Cell Science*. 2012; 125: 2017–2029.
- [99] Seri B, García-Verdugo JM, McEwen BS, Alvarez-Buylla A. Astrocytes give rise to new neurons in the adult mammalian hippocampus. *The Journal of Neuroscience*. 2001; 21: 7153–7160.
- [100] Varela-Nallar L, Alfaro IE, Serrano FG, Parodi J, Inestrosa NC. Wingless-type family member 5A (Wnt-5a) stimulates synaptic differentiation and function of glutamatergic synapses. *Proceedings of the National Academy of Sciences*. 2010; 107: 21164–21169.
- [101] Sousa KM, Villaescusa JC, Cajanek L, Ondr JK, Castelo-Branco G, Hofstra W, *et al.* Wnt2 regulates progenitor proliferation in the developing ventral midbrain. *The Journal of Biological Chemistry*. 2010; 285: 7246–7253.
- [102] Liebl FLW, McKeown C, Yao Y, Hing HK. Mutations in Wnt2 alter presynaptic motor neuron morphology and presynaptic protein localization at the *Drosophila* neuromuscular junction. *PLoS ONE*. 2010; 5: e12778.
- [103] Lin L, Lee VM, Wang Y, Lin JS, Sock E, Wegner M, *et al.* Sox11 regulates survival and axonal growth of embryonic sensory neurons. *Developmental Dynamics*. 2011; 240: 52–64.
- [104] Jankowski MP, Cornuet PK, McIlwrath S, Koerber HR, Albers KM. SRY-box containing gene 11 (Sox11) transcription factor is required for neuron survival and neurite growth. *Neuroscience*. 2006; 143: 501–514.
- [105] Jankowski MP, McIlwrath SL, Jing X, Cornuet PK, Salerno KM, Koerber HR, *et al.* Sox11 transcription factor modulates peripheral nerve regeneration in adult mice. *Brain Research*. 2009; 1256: 43–54.
- [106] Chang K, Bian M, Xia X, Madaan A, Sun C, Wang Q, *et al.* Posttranslational Modification of Sox11 Regulates RGC Survival and Axon Regeneration. *eNeuro*. 2021; 8: ENEURO.0358-20.2020.
- [107] Li Y, Struebing FL, Wang J, King R, Geisert EE. Different Effect of Sox11 in Retinal Ganglion Cells Survival and Axon Regeneration. *Frontiers in Genetics*. 2018; 9: 633.
- [108] Malin D, Sonnenberg-Riethmacher E, Guseva D, Wagener R, Aszódi A, Irintchev A, *et al.* The extracellular-matrix protein matrilin 2 participates in peripheral nerve regeneration. *Journal of Cell Science*. 2009; 122: 995–1004.
- [109] Bénardais K, Delfino G, Samama B, Devys D, Antal M, Ghandour M, *et al.* BBS4 protein has basal body/ciliary localization in sensory organs but extra-ciliary localization in oligodendrocytes during human development. *Cell and Tissue Research*. 2021; 385: 37–48.
- [110] Uyttingco CR, Williams CL, Xie C, Shively DT, Green WW, Ukhanov K, *et al.* BBS4 is required for intraflagellar transport coordination and basal body number in mammalian olfactory cilia. *Journal of Cell Science*. 2019; 132: jcs222331.
- [111] Ishii N, Wadsworth WG, Stern BD, Culotti JG, Hedgecock EM. UNC-6, a laminin-related protein, guides cell and pioneer axon migrations in *C. elegans*. *Neuron*. 1992; 9: 873–881.
- [112] Serafini T, Colamarino SA, Leonardo ED, Wang H, Bedington R, Skarnes WC, *et al.* Netrin-1 is required for commissural axon guidance in the developing vertebrate nervous system. *Cell*. 1996; 87: 1001–1014.
- [113] Furne C, Rama N, Corset V, Chédotal A, Mehlen P. Netrin-1 is a survival factor during commissural neuron navigation. *Proceedings of the National Academy of Sciences of the United States of America*. 2008; 105: 14465–14470.
- [114] Mount JG, Muzylak M, Allen S, Althnaian T, McGonnell IM, Price JS. Evidence that the canonical Wnt signalling pathway regulates deer antler regeneration. *Developmental Dynamics*. 2006; 235: 1390–1399.
- [115] Li Q, Wang M, Xue H, Liu W, Guo Y, Xu R, *et al.* Ubiquitin-Specific Protease 34 Inhibits Osteoclast Differentiation by Regulating NF- $\kappa$ B Signaling. *Journal of Bone and Mineral Research*. 2020; 35: 1597–1608.
- [116] Guo Y, Wang M, Zhang S, Wu Y, Zhou C, Zheng R, *et al.* Ubiquitin-specific protease USP34 controls osteogenic differentiation and bone formation by regulating BMP2 signaling. *The EMBO Journal*. 2020; 39: e105578.
- [117] Zhao F, Ma X, Qiu W, Wang P, Zhang R, Chen Z, *et al.* Mes-

enchymal MACF1 Facilitates SMAD7 Nuclear Translocation to Drive Bone Formation. *Cells*. 2020; 9: 616.

- [118] Su P, Yin C, Li D, Yang C, Wang X, Pei J, *et al.* MACF1 promotes preosteoblast migration by mediating focal adhesion turnover through EB1. *Biology Open*. 2020; 9: bio048173.
- [119] Qiu W, Ma X, Lin X, Zhao F, Li D, Chen Z, *et al.* Deficiency of Macf1 in osterix expressing cells decreases bone formation by Bmp2/Smad/Runx2 pathway. *Journal of Cellular and Molecular Medicine*. 2020; 24: 317–327.
- [120] Zheng HF, Tobias JH, Duncan E, Evans DM, Eriksson J, Paterson L, *et al.* WNT16 influences bone mineral density, cortical bone thickness, bone strength, and osteoporotic fracture risk. *PLoS Genetics*. 2012; 8: e1002745.
- [121] Movérare-Skrtic S, Henning P, Liu X, Nagano K, Saito H, Börjesson AE, *et al.* Osteoblast-derived WNT16 represses osteoclastogenesis and prevents cortical bone fragility fractures. *Nature medicine*. 2014; 20: 1279–1288.